

# Designed, Helical Protein Nanotubes with Variable Diameters from a Single Building Block

Jeffrey D. Brodin,<sup>†</sup> Sarah J. Smith,<sup>†</sup> Jessica R. Carr, and F. Akif Tezcan\*

Department of Chemistry & Biochemistry, UCSD, 9500 Gilman Drive, La Jolla, California 92093, United States

**S** Supporting Information

**ABSTRACT:** Due to their structural and mechanical properties, 1D helical protein assemblies represent highly attractive design targets for biomolecular engineering and protein design. Here we present a designed, tetrameric protein building block,  $Zn_8R_4$ , which assembles via Zn coordination interactions into a series of crystalline, helical nanotubes whose widths can be controlled by solution conditions. X-ray crystallography and transmission electron microscopy (TEM) measurements indicate that all classes of protein nanotubes are constructed through the same 2D arrangement of  $Zn_8R_4$  tetramers held together by Zn coordination. The mechanical properties of these nanotubes are correlated with their widths. All  $Zn_8R_4$  nanotubes are found to be highly flexible despite possessing crystalline order, owing to their minimal interbuilding-block interactions mediated solely by metal coordination.

A major goal in nanotechnology is the bottom-up design and construction of self-assembled materials that combine the structural order, dynamicity, and functional properties of natural protein assemblies.<sup>1,2</sup> Of particular interest are one-dimensional, helical architectures with hollow interiors, which in nature fulfill a large number of biomechanical roles such as the formation of the cytoskeleton,<sup>3</sup> molecular transport and cell division,<sup>4,5</sup> cell motility,<sup>6</sup> infection,<sup>7,8</sup> endocytosis,<sup>9,10</sup> and compartmentalization.<sup>11</sup> Invariably, all of these biological architectures are assembled from small (<10 nm) protein building blocks that polymerize through noncovalent interactions in a helical symmetry. This mode of assembly, endows natural, 1D protein architectures with the ability to rapidly polymerize or depolymerize and to adapt their structures in response to external stimuli while retaining high mechanical/chemical stability. These properties of biological nanotubes, along with their inherent directionality, chirality, long-range and short-range periodicity, and high surface area-to-volume ratios, render them as highly attractive molecular templates and design targets.<sup>12,13</sup>

While peptide-based building blocks have shown promise for constructing helical superstructures,<sup>3,12,14–19</sup> successes in the design of tubular assemblies from protein synthons have been limited to the use of physical methods,<sup>20–23</sup> assembly under harsh conditions that alter the structure of the protein subunits,<sup>24</sup> or to the use of natively ring-shaped proteins, which can be manipulated to stack into tubes.<sup>25</sup> We recently established that the simultaneous strength, directionality, and reversibility of metal coordination interactions can be exploited to direct the

formation of small protein building blocks into discrete oligomers or highly ordered 1-, 2-, and 3D architectures.<sup>26–31</sup> These assemblies are distinguished from many other designed supramolecular protein architectures by their stimuli-responsiveness. Because metal–protein interactions are inherently tunable (through metal concentration, identity, oxidation state, or solution pH), it follows that the structures and assembly states of metal-directed protein architectures can also be modulated by external stimuli. Accordingly, we present here the metal-directed assembly of a designed protein building block into a series of crystalline, helical nanotubes, whose diameters and structure-dependent mechanical properties can be varied through solution conditions that modulate metal–protein interactions.

From a retrosynthetic perspective, a 1D helical tube can be considered as an anisotropic (i.e., rectangular) 2D sheet wrapped around a cylinder with longitudinal and lateral growth axes (Figure S1). Such a rectangular 2D sheet can be constructed from self-assembling  $D_2$  symmetric building blocks that similarly possess bidirectional symmetry in the 2D plane. If the interactions between these building blocks can be controlled (thermodynamically or kinetically) through external means, it should be possible to modulate the magnitude of anisotropy between the longitudinal and lateral growth directions, thereby controlling the widths or the aspect ratios of the resulting tubes. Previously, we reported on the construction of  $D_2$  symmetric assemblies of the monomeric protein cytochrome  $cb_{562}$  through  $Zn^{2+}$  coordination.<sup>32,33</sup> Here, we considered that these tetrameric scaffolds themselves can be used as building blocks for assembling anisotropic 2D sheets (and thereby 1D nanotubes), as they feature two sets of weakly metal chelating motifs on their external surfaces to promote bidirectional growth: Motif 1, the bidentate combination of Glu8 and Asp12 carboxylates; Motif 2, the tridentate combination of Ala1 N-terminal amine and carbonyl oxygen and Glu39 carboxylate (Figures 1 and 2). Both motifs were observed in several crystal structures to be capable of mediating latticepacking interactions through  $Zn^{2+}$  coordination.<sup>34</sup>

As a starting point for building a stable  $D_2$  symmetric building block, we used a cyt  $cb_{562}$  variant (RIDC3), which was previously designed to form Zn-mediated dimers that further assembled into 1-, 2-, and 3D arrays.<sup>26,27</sup> RIDC3 was engineered with a Cys residue at position 96 (informed by earlier work),<sup>33</sup> such that it could be prepared as a covalent C96–C96 linked dimer (Figures 1a and S2). A His residue was then incorporated in position 59 in addition to pre-existing metal-coordinating residues on RIDC3,

Received: June 3, 2015

Published: August 10, 2015

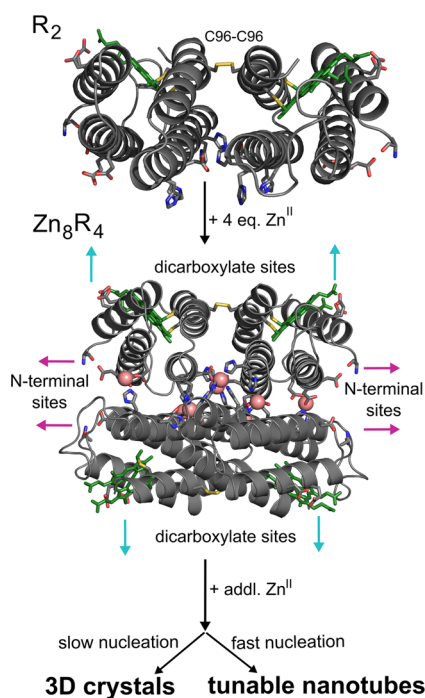


**Figure 1.** Proposed Zn-mediated assembly of a disulfide-linked protein dimer ( $R_2$ ) into a closed,  $D_2$  symmetric tetramer ( $Zn_8R_4$ ), which acts as a synthon for larger supramolecular architectures upon further Zn coordination. Heme cofactors are shown as green sticks; they have been omitted in later figures for clarity.

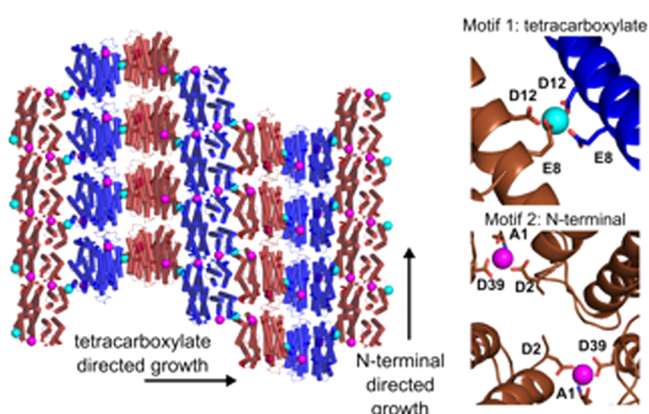


**Figure 2.** Crystallographic characterization of  $Zn_8R_4$ . Motif 1 (cyan spheres) and Motif 2 (magenta spheres) coordination sites promote intertetramer assembly and the formation of higher order arrays. Protein tetramers are alternatively colored to highlight 2D arrangement. See Figure S4 for a detailed view of an individual  $Zn_8R_4$  tetramer.

such that the disulfide-linked dimers would lock into the desired  $D_2$  tetramer via coordination by eight  $Zn^{2+}$  ions ( $Zn_8$ :<sup>H59/C96</sup>RIDC3<sub>4</sub>, Figure 1b). The dimeric, metal-free dimer is hereafter referred to as  $R_2$  and the metal-bound tetramer as  $Zn_8R_4$ .

To probe whether  $Zn_8R_4$  properly forms and can self-assemble into planar sheets, we first set out to produce single 3D crystals by Zn-directed self-assembly. Following a previously described strategy,<sup>26</sup> we were able to assemble hexagonal, diffraction quality crystals of  $Zn_8R_4$  in bulk solution by including high concentrations of the metal-coordinating buffer TRIS, which lowers the effective free Zn concentration and slows the nucleation rate of crystals (Figure S3). The 2.3 Å resolution

crystal structure (Table S1,  $P6_122$ ,  $52.9 \times 52.9 \times 257.1$  Å, PDB ID SBU7) confirmed the formation of the desired  $D_2$  symmetric tetramers, the pair of C96–C96 disulfide bonds and the two sets of four, internal Zn-coordination sites (Figures 2 and S4). The examination of the lattice revealed that the  $Zn_8R_4$  units could indeed form 2D arrays through Zn coordination by Motif 1 and Motif 2 (Figure 2). While these 2D arrays are not flat (owing to the  $6_1$  screw axis that runs along the 2D  $bc$  plane) and not every tetramer has its external Zn-coordination motifs occupied, the sheets are contiguously linked by  $Zn^{2+}$  ions and the two motifs propagate self-assembly in orthogonal directions as intended. Further growth of these 2D arrays into 3D crystals is directed by  $Zn^{2+}$  ions oriented perpendicular to their surfaces (Figure S5).

Whereas the metal-mediated assembly of large 3D crystalline arrays is promoted under slow nucleation/growth conditions (low pH, low effective metal concentration), the formation of 1D nanotubes are expected to be favored when the nucleation is rapid (high pH, high effective metal concentration).<sup>26</sup> In initial experiments for forming 1D nanotubes, we first incubated  $R_2$  dimers with a 5-fold molar excess of  $Zn^{2+}$  at pH 7.5 in a nonmetal chelating buffer (MOPS) to preform the  $Zn_8R_4$  tetramers, which was followed by the addition of another 5-fold excess of  $Zn^{2+}$ . This treatment resulted in the rapid formation of uniform, helical protein nanotubes that were  $48 \pm 3$  nm wide (Class I) based on negative-stain (ns) TEM (Figures 3, S6, and S7). In contrast, the

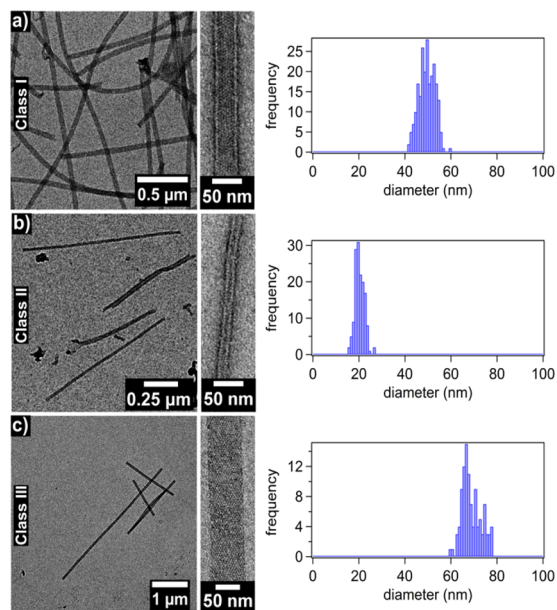


**Figure 3.** ns TEM images of  $Zn_8R_4$  nanotubes.

addition of 10-fold excess  $Zn^{2+}$  in the second step produced significantly thinner, monodisperse nanotubes (Class II) with a diameter of  $20 \pm 2$  nm. Stepwise  $Zn^{2+}$  addition was critical for forming monodisperse populations of nanotubes. When 10-fold excess of  $Zn^{2+}$  was directly added to the  $R_2$  dimer solution without the preincubation step, we observed the formation of amorphous aggregates in addition to Type I nanotubes. When a larger excess of  $Zn^{2+}$  was added without the preincubation step, only amorphous aggregates were observed. The formation of these disordered species is likely due to presence of multiple possible Zn-mediated assembly modes of the  $R_2$  dimers and the formation of kinetically trapped amorphous aggregates. The above experiments were repeated at pH 6.5 (in noncoordinating,

MES buffer), where the metal–protein coordination interactions (particularly that by the N-terminal amine of Motif 2) would be expected to be weaker. As at pH 7.5, the stepwise addition of 5 + 5-fold excess of  $\text{Zn}^{2+}$  to the  $\text{R}_2$  solution yielded the Class I nanotubes, and the direct addition of 20-fold excess  $\text{Zn}^{II}$  resulted in heterogeneous aggregates. In contrast, the direct addition of 10-fold excess  $\text{Zn}^{2+}$  led to the formation of yet another class (Class III) of highly ordered, helical nanotubes that were  $68 \pm 4$  nm wide. The observation that the structural outcome of self-assembly is dependent on the sequence of Zn addition indicates that the formation of different classes of  $\text{Zn}_8\text{R}_4$  nanotubes is kinetically governed. We postulate that the decisive, structural-determining steps occur during initial nucleation/growth stages.

For structural analysis of  $\text{Zn}_8\text{R}_4$  nanotubes, we first took advantage of the fact that some Class I nanotubes presented frayed ends that possessed a flat, single-layered 2D morphology (Figure 4). The reconstructed TEM images from both the tubular

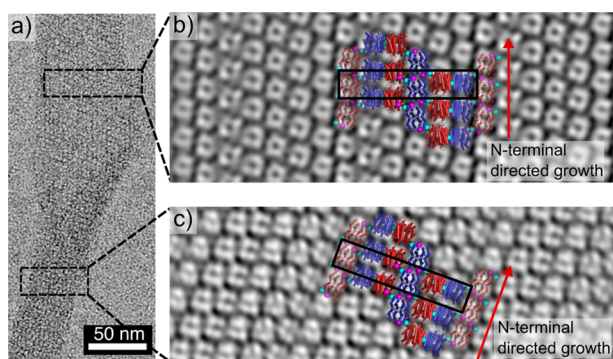


**Figure 4.** ns TEM characterization of  $\text{Zn}_8\text{R}_4$  arrays. (a) Single Class I nanotube with tubular (bottom) and frayed (top) segments. (b,c) 2D reconstructions of tubular (b) and frayed (c) regions of a single nanotube. The crystallographically characterized 2D pattern of  $\text{Zn}_8\text{R}_4$  molecules is superimposed onto the TEM reconstructions. The slight mismatch between the crystallographic model and TEM reconstruction in (b) is likely due to the curved nature of the 2D arrays, which is accounted for by the curvature of the tubes.

and the flat regions of the Class I nanotubes revealed compact structures with dimensions similar to the  $\text{Zn}_8\text{R}_4$  tetramers (Figures S8 and S9), which were clearly distinct from those observed in reconstructions of RIDC3 nanotubes (Figure S10). These tetramers are arranged into unit cells, each of which consist of six subunits, with dimensions ( $52 \text{ \AA} \times 270 \text{ \AA}$ , black boxes in Figures 4b,c) that are very similar to those seen in the 3D crystals. Indeed, the 2D packing arrangement of  $\text{Zn}_8\text{R}_4$  tetramers observed in the X-ray crystal structure fits reasonably well in the TEM-derived molecular pattern. An analysis of the Class II and Class III nanotubes indicates that they also contain the same arrangement (Figures S11 and S12). These results strongly suggest that the Zn coordination interactions that mediate the formation of the three classes of  $\text{Zn}_8\text{R}_4$  nanotubes are the same as those present in the 3D crystal lattice. To provide further evidence that the nanotubes have a similar arrangement of tetramers as in 3D crystals, we constructed a structural model of the thinnest (Class II) tubes. This model indicates that it is possible to build a contiguous, well-packed, helical tube with the expected 15 nm diameter using the crystallographically observed intertetramer interaction modalities (Figure 5). According to this model, the Zn–Motif 1 interactions point along the lateral tube axis, whereas the Zn–Motif 2 interactions are oriented longitudinally, suggesting that the width/aspect ratios of the

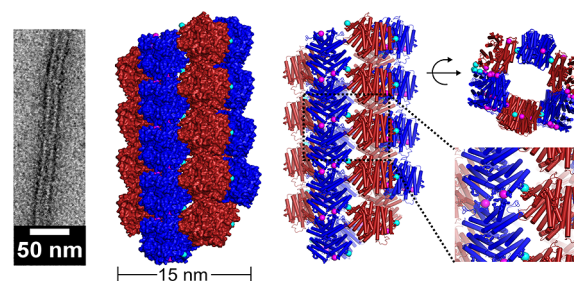


**Figure 5.** Structural model for Class II nanotubes.

$\text{Zn}_8\text{R}_4$  nanotubes must be influenced by the differential Zn coordination thermodynamics/kinetics of Motif1- and Motif2-mediated interactions. Specifically, deprotonation of the N-terminal amine of Motif 2 at higher pH values apparently results in a larger difference between the interaction strengths of the two coordination motifs and correspondingly thinner nanotubes.

Various structural and derived mechanical properties of the  $\text{Zn}_8\text{R}_4$  nanotubes are summarized in Table 1. A comparison of the

**Table 1. Structural and Derived Mechanical Properties of the  $\text{Zn}_8\text{R}_4$  Tubes**

	Class I	Class II	Class III
Width (ns) (nm)	$48 \pm 3$	$20 \pm 2$	$68 \pm 4$
Width (cryo) (nm)	$25 \pm 2$	$15 \pm 1$	$46 \pm 3$
Persistence length (ns) ( $\mu\text{m}$ )	$28.2 \pm 0.3$	$15.1 \pm 0.3$	$64.5 \pm 1.1$
Persistence length (cryo) ( $\mu\text{m}$ )	$16.4 \pm 0.2$	$8.8 \pm 0.4$	$17.8 \pm 0.4$
Estimated Young's modulus (ns) (MPa)	1.4	15	1.1
Estimated Young's modulus (cryo) (MPa)	0.8	25	0.3

cryoEM and negative-stain TEM (Figures S13 and S14) analyses indicates that the wide Class III tubes undergo significant flattening by uranyl-acetate staining/drying. In contrast, the thin Class II nanotubes were not greatly affected by this treatment, which can be ascribed to their higher density of protein packing that affords resistance to lateral compression. The persistence lengths of the nanotubes were calculated using the recently published program FiberApp (Figure S15)<sup>35</sup> and found to be consistently higher for uranyl-stained samples compared to cryoEM samples. As judged by cryoEM data, the thinnest Class II tubes are also the most flexible with a persistence length ( $9 \mu\text{m}$ ) that is approximately half that of the widest Class III tubes ( $18 \mu\text{m}$ ). These values are similar to the persistence lengths of actin filaments ( $17.7 \mu\text{m}$ )<sup>36</sup> and significantly higher than that of double-stranded DNA ( $50 \text{ nm}$ ),<sup>37</sup> but considerably lower than that of microtubules ( $5.2 \text{ mm}$ ).<sup>36</sup> It is notable that the  $\text{Zn}_8\text{R}_4$  nanotubes are similar to microtubules ( $24 \text{ nm}$  outer and  $12 \text{ nm}$  inner diameter) in terms of their dimensions. We posit that the higher stiffness of microtubules arises from their considerably more extensive, highly evolved intermonomer interfaces ( $\sim 3000 \text{ \AA}^2$  buried surface area)<sup>38</sup> compared to those in the  $\text{Zn}_8\text{R}_4$  nanotubes that are mediated solely by metal coordination with no complementary noncovalent interactions. The Young's moduli of the  $\text{Zn}_8\text{R}_4$  nanotubes can be estimated from the persistence lengths using eq 1.<sup>39,40</sup>

$$E = (4k_B TP)/(\pi a^4) \quad (1)$$

where  $k_B$  is the Boltzmann constant,  $T$  is temperature,  $P$  is persistence length, and  $a$  is the radius of the tubes. The estimated

Young's moduli serve to roughly understand how these artificial nanotubes compare to those found in nature, with the caveat that additional experiments would need to be performed to more accurately determine these values. The range of values obtained (from 0.3 MPa for Class III to 25 MPa for Class II) are comparable to values determined for soft protein fibers such as fibrin (1–10 MPa) or elastin (1 MPa) and much less stiff than microtubules (1000–1500 MPa).<sup>39</sup> These data again indicate that the Zn<sub>8</sub>R<sub>4</sub> nanotubes are highly flexible, yet simultaneously possess crystalline order. Under certain conditions, we observed the formation of unique, multiwalled nanotubes alongside Class I nanotubes (Figure S16). Additionally, after incubations of >1 month in solution, we observed the bundling of the Class II nanotubes, reminiscent of actin filament aggregates (Figure S17).<sup>41</sup> The formation of both of these superstructures is likely promoted by the presence of unsaturated Zn sites on the surfaces of the nanotubes and may provide a means to increase their mechanical stiffness. Regardless of their flexibility, Zn<sub>8</sub>R<sub>4</sub> nanotubes are highly stable and persist in solution at room temperature for at least one year (Figure S18).

In conclusion, we have demonstrated the implementation of metal coordination chemistry to generate multiple well-defined, nanoscale architectures with different structural/mechanical properties from a single, designed protein building block. Typically, protein design approaches have aimed to construct singular structural targets that represent the thermodynamically most favored molecular arrangement formed under equilibrium conditions. This scenario contrasts with many biological self-assembly processes that proceed under nonequilibrium conditions and may yield different structural outcomes based on the environmental conditions or energy input.<sup>2</sup> In analogy to such natural, nonequilibrium processes, our study shows that it is possible to kinetically dictate protein self-assembly through the use of externally tunable intermolecular interactions such as metal coordination.

## ■ ASSOCIATED CONTENT

### Supporting Information

The Supporting Information is available free of charge on the ACS Publications website at DOI: 10.1021/jacs.5b05755.

Experimental details for protein characterization, table for crystallographic data collection/refinement, and TEM analysis (PDF)

## ■ AUTHOR INFORMATION

### Corresponding Author

\*tezcan@ucsd.edu

### Author Contributions

†These authors contributed equally to this work.

### Notes

The authors declare no competing financial interest.

## ■ ACKNOWLEDGMENTS

This work was supported by the US Department of Energy (DOE) (Division of Materials Sciences, Office of Basic Energy Sciences, Award DE-FG02-10ER46677 to F.A.T.). Use of the Stanford Synchrotron Radiation Lightsource, SLAC National Accelerator Laboratory, is supported by the U.S. DOE, Office of Science, Office of Basic Energy Sciences under Contract No. DE-AC0276F00515.

## ■ REFERENCES

- (1) Whitesides, G. M.; Mathias, J. P.; Seto, C. T. *Science* **1991**, *254*, 1312.
- (2) Mann, S. *Angew. Chem., Int. Ed.* **2008**, *47*, 5306.
- (3) Dominguez, R.; Holmes, K. C. *Annu. Rev. Biophys.* **2011**, *40*, 169.
- (4) Nogales, E. *Annu. Rev. Biophys. Biomol. Struct.* **2001**, *30*, 397.
- (5) Wade, R. H.; Chretien, D.; Job, D. *J. Mol. Biol.* **1990**, *212*, 775.
- (6) Terashima, H.; Kojima, S.; Homma, M. *Int. Rev. Cell Mol. Biol.* **2008**, *270*, 39.
- (7) Loquet, A.; Sgourakis, N. G.; Gupta, R.; Giller, K.; Riedel, D.; Goosmann, C.; Griesinger, C.; Kolbe, M.; Baker, D.; Becker, S.; Lange, A. *Nature* **2012**, *486*, 276.
- (8) Basler, M.; Pilhofer, M.; Henderson, G. P.; Jensen, G. J.; Mekalanos, J. J. *Nature* **2012**, *483*, 182.
- (9) Stowell, M. H.; Marks, B.; Wigge, P.; McMahon, H. T. *Nat. Cell Biol.* **1999**, *1*, 27.
- (10) Mears, J. A.; Ray, P.; Hinshaw, J. E. *Structure* **2007**, *15*, 1190.
- (11) Stubbs, G.; Kendall, A. *Adv. Exp. Med. Biol.* **2012**, *726*, 631.
- (12) Reches, M.; Gazit, E. *Science* **2003**, *300*, 625.
- (13) Zhang, S. *Nat. Biotechnol.* **2003**, *21*, 1171.
- (14) Egelman, E. H.; Xu, C.; DiMaio, F.; Magnotti, E.; Modlin, C.; Yu, X.; Wright, E.; Baker, D.; Conticello, V. P. *Structure* **2015**, *23*, 280.
- (15) Ghadiri, M. R.; Choi, C. *J. Am. Chem. Soc.* **1990**, *112*, 1630.
- (16) Hamley, I. W. *Angew. Chem., Int. Ed.* **2007**, *46*, 8128.
- (17) O'Leary, L. E. R.; Fallas, J. A.; Bakota, E. L.; Kang, M. K.; Hartgerink, J. D. *Nat. Chem.* **2011**, *3*, 821.
- (18) Sharp, T. H.; Bruning, M.; Mantell, J.; Sessions, R. B.; Thomson, A. R.; Zaccari, N. R.; Brady, R. L.; Verkade, P.; Woolfson, D. N. *Proc. Natl. Acad. Sci. U. S. A.* **2012**, *109*, 13266.
- (19) Tarabout, C.; Roux, S.; Gobeaux, F.; Fay, N.; Pouget, E.; Meriadec, C.; Ligeti, M.; Thomas, D.; Ijsselstijn, M.; Besselièvre, F.; Buisson, D. A.; Verbavatz, J. M.; Petitjean, M.; Valery, C.; Perrin, L.; Rousseau, B.; Artzner, F.; Paternostre, M.; Cintrat, J. C. *Proc. Natl. Acad. Sci. U. S. A.* **2011**, *108*, 7679.
- (20) Hou, S.; Wang, J.; Martin, C. R. *Nano Lett.* **2005**, *5*, 231.
- (21) Lu, G.; Ai, S.; Li, J. *Langmuir* **2005**, *21*, 1679.
- (22) Lu, G.; Komatsu, T.; Tsuchida, E. *Chem. Commun.* **2007**, 2980.
- (23) Qu, X.; Komatsu, T. *ACS Nano* **2010**, *4*, 563.
- (24) Lara, C.; Handschin, S.; Mezzenga, R. *Nanoscale* **2013**, *5*, 7197.
- (25) Ballister, E. R.; Lai, A. H.; Zuckermann, R. N.; Cheng, Y.; Mougous, J. D. *Proc. Natl. Acad. Sci. U. S. A.* **2008**, *105*, 3733.
- (26) Brodin, J. D.; Ambroggio, X. I.; Tang, C.; Parent, K. N.; Baker, T. S.; Tezcan, F. A. *Nat. Chem.* **2012**, *4*, 375.
- (27) Brodin, J. D.; Carr, J. R.; Sontz, P. A.; Tezcan, F. A. *Proc. Natl. Acad. Sci. U. S. A.* **2014**, *111*, 2897.
- (28) Salgado, E. N.; Ambroggio, X. I.; Brodin, J. D.; Lewis, R. A.; Kuhlman, B.; Tezcan, F. A. *Proc. Natl. Acad. Sci. U. S. A.* **2010**, *107*, 1827.
- (29) Radford, R. J.; Brodin, J. D.; Salgado, E. N.; Tezcan, F. A. *Coord. Chem. Rev.* **2011**, *255*, 790.
- (30) Radford, R. J.; Tezcan, F. A. *J. Am. Chem. Soc.* **2009**, *131*, 9136.
- (31) Song, W. J.; Tezcan, F. A. *Science* **2014**, *346*, 1525.
- (32) Salgado, E. N.; Faraone-Mennella, J.; Tezcan, F. A. *J. Am. Chem. Soc.* **2007**, *129*, 13374.
- (33) Brodin, J. D.; Medina-Morales, A.; Ni, T.; Salgado, E. N.; Ambroggio, X. I.; Tezcan, F. A. *J. Am. Chem. Soc.* **2010**, *132*, 8610.
- (34) PDB IDs 4JEB, 3TOM, 3QVY, 3M4B, and 3M4C.
- (35) Usov, I.; Mezzenga, R. *Macromolecules* **2015**, *48*, 1269.
- (36) Gittes, F.; Mickey, B.; Nettleton, J.; Howard, J. *J. Cell Biol.* **1993**, *120*, 923.
- (37) Bloom, K. S. *Chromosoma* **2008**, *117*, 103.
- (38) Löwe, J.; Li, H.; Downing, K. H.; Nogales, E. *J. Mol. Biol.* **2001**, *313*, 1045.
- (39) Guthold, M.; Liu, W.; Sparks, E. A.; Jawerth, L. M.; Peng, L.; Falvo, M.; Superfine, R.; Hantgan, R. R.; Lord, S. T. *Cell Biochem. Biophys.* **2007**, *49*, 165.
- (40) Trachtenberg, S.; Hammel, I. In *Microscopy: Science, Technology, Applications and Education*; Mendez-Villas, A., Diaz, J., Eds.; Formatex Research Center: Badajoz, Spain, 2010; Vol. 3.
- (41) Bremer, A.; Aebi, U. *Curr. Opin. Cell Biol.* **1992**, *4*, 20.